

## Author's response to anonymous referee comments

Below we provide in blue-colored font a point-by-point reply to each comment.

### Anonymous Referee #1

I would like to congratulate the authors on the development of a novel and useful instrument for linking topographic features on bulk systems to ice growth. The results are clearly presented and the manuscript is well written. Nevertheless, I have a few comments listed below.

We thank the referee for the kind words regarding our novel approach to studying ice growth, as well as the referee's insightful comments.

#### General comments:

The paper initially describes the technique as an instrument for elucidating atmospheric ice formation. However, the primary focus of the results are about ice growth and propagation on the feldspar mineral. Although this is an interesting observation and result, it is not very atmospherically relevant. As in the atmosphere, the aerosols acting as INPs are between approximately 50 and 10000 nm. Therefore, it is likely that individual droplets would not exist on the surface of the aerosol particle. Rather, the entire aerosol would be immersed in a cloud droplet above water saturation and the ice nucleation event would cause the entire droplet to freeze. This renders the step height analysis unnecessary for atmospheric ice formation. I think this should be more clearly presented in the manuscript.

We concur with the referee that our observations on extended feldspar surfaces cannot straightforwardly applied to atmospheric conditions. We agree that most aerosol particles are typically completely immersed in a cloud droplet already at very modest supersaturations. We address this issue by adding text in the manuscript to: (1) Clarify at the outset that and why we are looking at extended substrates, thus not raising the not-to-be-fulfilled expectation that we examine realistic aerosol particles. (2) Describe more precisely the atmospheric conditions for which we believe our results might be relevant. Specifically, we:

Changed the first sentence in the abstract to: *"We developed a method for examining ice formation on solid substrates exposed to cloud-like atmospheres."*

Before the last sentence of the introduction we added: *"While studying aerosol particles collected from the atmosphere would provide a more direct connection to atmospheric conditions. The typically complex structure and chemistry of these particles often precludes identifying the individual nanoscale processes that are important. For this study, instead, we choose extended flat substrates of known composition on which the role of individual topographic features can be examined."*

In first sentence of paragraph 2.1.1. changed *"To create cloud-like conditions"* to *"To create a cloud-like atmosphere"*.

In the discussion and outlook section we added the following two statements:

*"This process can be viewed as an extension of the pore condensation and freezing mechanism (Christenson 2013; David et al. 2019; Fukuta 1966; Marcolli 2014; Pach and Verdaguer 2019) to higher humidity."*

*"Typically, most aerosol particles are completely immersed in a cloud droplet already at very modest supersaturations. As discussed in detail in (Fridde and Thürmer 2019a), the step-facilitated mechanism described above is expected to be relevant when a cavity-free feldspar particle, initially devoid of ice, is suspended in air colder than -20°C that becomes slowly saturated. According to Fletcher's estimate (Fletcher 1962; Pruppacher and Klett 1997) that a humidity of  $RH_w > 130\%$  is required for a measurable nucleation rate of water droplets with a contact angle of  $\approx 45^\circ$  on a planar insoluble substrate. Hence*

condensation of supercooled water will be confined to step edges, where the water will freeze rapidly, thus initiating ice formation.”

Nevertheless, the step height analysis is potentially an interesting and important result for the material science, biomedical and food preservation fields. Perhaps the authors should present the step height analysis in reference to those fields.

Following the referee’s suggestion we added to following statement to the discussion and outlook section: *“In the discussed example of ice formation, the step-height analysis is used to corroborate the involvement of the liquid phase of water during the observed rapid formation and propagation of ice on feldspar, while the link between surface-step height and the ability of an isolated aerosol particle to initiate ice nucleation is neither direct nor obvious. Nevertheless, such step-height analysis might benefit future studies in fields of material science, like corrosion and aircraft icing (Gent, Dart, and Cansdale 2000; Kreder et al. 2016), where the behavior of the examined materials is affected by the abundance of surface steps.”*

Although it is discussed that certain sites repeatedly nucleated ice while others lost that ability, it would be nice to show some examples of the types of sites that retained or lost their ice nucleating ability. For example, do they differ in geometry, location on the mineral surface etc.

We did not perform an exhaustive study on the sites that lose or gain the ability to nucleate ice. With our optically limited spatial resolution of the ice crystals we are unable to decisively make a statement on the local surface structure (sub 10 nm) where nucleation occurs.

Do the crystals that emerge from pits below water saturation or protrusions above water saturation have the same orientation as discussed in the Kiselev et al., (2017) study?

We did not observe the regularity in crystal orientation as reported in the Kiselev study. We added at the end of section 4: *“Our data neither reveal nor rule out any preferred crystal orientation of the observed ice structures.”*

Minor Comments:

What is the resolution of the AFM? What is the tip width and how does this affect the mapping of the topographic features?

We did not characterize the radii of the AFM tips we used. Although the manufacturer specifies the tip radii is < 10 nm, typically over extended use situations the tip radius is approximately 20 nm, putting the theoretical lateral resolution at about 4nm, while the vertical resolution is atomic. That said, the data used in our mapping is constructed of individual scans of 512x512 pixels covering 100x100  $\mu\text{m}^2$ . This limits the spatial resolution to the pixel size of 195 nm. We included the tip model and vendor in section 2.2.

What is the temperature uncertainty of the thermistor? Is there an impact of the temperature measurement occurring below the standoff stage rather than below the sample itself (see Fig. 1)?

The inherent error in the thermistor reading is negligible (less than 0.1 C) compared to the uncertainty introduced by the sensor placement below the sample. In the setup in for these experiments we do not

use a sensor within the sample volume, however the flux of cold gas impinging the base of the sample plate is 20 times greater than the flux flowing over the top of the sample. Thus, only a small differential is expected between the sample base and sample volume temperatures. We revisited our temperature measurements and found a slight error in our original reporting of the temperature of the sample plate. Our measurements of the sample plate temperature were on average  $-29.5 \pm 0.2$  °C, where the error is the standard deviation of the readings over 9 runs. We take a conservative estimate to place the error at  $\pm 0.5$  °C. We have included this revised temperature and error throughout the paper, as well as adjusted the estimated AHin values accordingly.

What are the uncertainties in the iced step height analysis? Please add error bars to the Fig. 6. Is there a reason that the largest step heights have a lower iced fraction above 0.75 AHin or is this due to the uncertainty of calculating the iced fraction of a step. This result is in direct conflict with the statement that higher iced steps would retain ice longer than shorter steps (see discussion and outlook).

Uncertainty in histogram data is difficult to define without a priori knowledge of the distribution, and therefore the variance of a given bin. The noise observed in the curves for large humidities at large step heights arises from the random nature of ice coverage and limited data. The order of step icing, and in turn local dehydration, is random in each experiment. Therefore, in some runs a section of steps will be dehydrated, while in others those same steps will become iced. Since tall step heights are present in fewer numbers this random dehydration path can remove a noticeable portion of those steps from the overall counts of iced steps. We included the following sentence in the caption to figure 6, "Fluctuations in the ice fraction curves, particularly at high AHin and large steps, reflect the random dehydration of some larger step heights which are present in far fewer numbers than smaller step heights."

It is not stated how the humidity would be calibrated at other temperatures? Would the AHin be increased until water is observed and then this be used as 100 % RH in the cell?

The reviewer is correct, the humidity would have to be re-calibrated for a different temperature.

I understand that once droplets are formed, the humidity would drop in the chamber, but at the highest AHin used in the study  $\sim 200$  % RH, do the droplets continue to grow/merge? As mentioned in the general comments, the experiments conducted above water saturation are investigating ice growth. Please make this clearer on page 5 line 11.

The actual humidity within the cell volume local to the viewing area is unknown and must be well below 200 % RH. As seen in the accompanying videos, in most areas the ice forms before the droplets are able to grow/merge to an appreciable size. We have changed this sentence to read, "Above saturation, we observe a very different pathway to ice formation." Where we removed "mode of" to distinguish from direct observation of ice nucleation.

#### Detailed comments:

Page 2 Line 5: Please add Pach and Verdaguer, (2019) We have now added this reference twice in the experimental results section 3.

Page 2 line 16: Remove "however" as this confuses the sentence and move the citations to the end of the sentence. Thank you for the suggestion, we have made this change.

Section 2.1.1 please reference Figure 1. Thank you, this is called out in the first sentence of section 2.1.1.

Section 2.1.1 on page 3 line 10 is not numbered correctly. Please change to 2.1.2 [Thank you, we have corrected this.](#)

Page 3 line 16: Capitalize “figure” [Thank you, we have corrected this.](#)

Page 3 line 24-26: This sentence seems unnecessary here especially as it is not explored in this study. Either reformulate to state that in theory this would be an additional advantage or remove.

*We reformulated this sentence to: “The last point has the potential benefit of keeping the AFM tip near the same temperature as the sample surface, allowing, in principle, to image ice on the sample surface without raising their temperature (not explored here).”*

Page 5 line 3: Please add appropriate references for ice formation from capillary condensation such as: Campbell et al., (2017); Campbell and Christenson, (2018); David et al., (2019); Marcolli, (2014); Pach and Verdaguer, (2019)

[Thank you, we have added the following appropriate references here: \(Christenson 2013; David et al. 2019; Fukuta 1966; Marcolli 2014; Pach and Verdaguer 2019\)](#)

Page 6 line 5: numbering of section is off, change to 4.2. [Thank you, we have corrected this.](#)

Page 6 line 27: please change ice formation to ice growth [We have made the change.](#)

#### References:

- Campbell, J. M. and Christenson, H. K.: Nucleation- and Emergence-Limited Growth of Ice from Pores, *Phys. Rev. Lett.*, 120(16), 165701, doi:10.1103/PhysRevLett.120.165701, 2018.
- Campbell, J. M., Meldrum, F. C. and Christenson, H. K.: Observing the formation of ice and organic crystals in active sites, *Proc. Natl. Acad. Sci.*, 114(5), 810–815, 2017.
- David, R. O., Marcolli, C., Fahrni, J., Qiu, Y., Sirkin, Y. A. P., Molinero, V., Mahrt, F., Brühwiler, D., Lohmann, U. and Kanji, Z. A.: Pore condensation and freezing is responsible for ice formation below water saturation for porous particles, *Proc. Natl. Acad. Sci.*, 116(17), 8184–8189, doi:10.1073/pnas.1813647116, 2019.
- Kiselev, A., Bachmann, F., Pedevilla, P., Cox, S. J., Michaelides, A., Gerthsen, D. and Leisner, T.: Active sites in heterogeneous ice nucleation – The example of K-rich feldspars, *Science*, 355(6323), 367–371, doi:10.1126/science.aai8034, 2017.
- Marcolli, C.: Deposition nucleation viewed as homogeneous or immersion freezing in pores and cavities, *Atmos Chem Phys*, 14(4), 2071–2104, doi:10.5194/acp-14-2071-2014, 2014.
- Pach, E. and Verdaguer, A.: Pores Dominate Ice Nucleation on Feldspars, *J. Phys. Chem. C*, 123(34), 20998–21004, doi:10.1021/acs.jpcc.9b05845, 2019.

## Anonymous Referee #2

The authors have assembled an experimental setup to grow ice crystals on a sample surface and developed a method to locate where ice forms to investigate the topographical features on the underlying surface by atomic-force microscopy. While the setup could prove useful to study ice growth on surfaces, the intended use to study ice nucleation mechanisms requires a higher vertical resolution to detect small ice crystals and pinpoint the location of ice active sites. In addition, much better control of temperature and relative humidity in the mixing chamber is needed. I think such could be achieved and encourage the authors to improve the setup towards this direction.

We thank the reviewer for their detailed review of our manuscript and helpful comments.

We would like to clarify that our manuscript is intended to detail our approach of collocating ice formation/growth locations observed optically to the sample surface structure observed by AFM. If the interpretation is that we are monitoring ice formation with AFM, we apologize for the lack of clarity and emphasize that we only observe ice optically. We agree that with optical observation, which is ultimately wavelength-limited to at least a micron, it is impossible to pinpoint ice nucleation sites with the necessary resolution of less than 10 nm. Other approaches in the literature that have ostensibly studied ice nucleation have a similar resolution limit due to the risk of beam damage. The ESEM approach also does not control the humidity but infers the local humidity around a growing ice crystal through relating the ice growth rate to the local supersaturation. This calculation can be carried out in our work as well, but due to the network of ice which rapidly forms on the surface, the humidity varies substantially across the surface and with time. Determining a representative humidity at these length-scales is not trivial and is obviously not a number but a landscape. We respectfully contend that the main message of the paper stands without investigating the humidity in great detail at this stage in development. Afterall, we are not studying kinetics of ice nucleation or crystal growth where the exact supersaturation is necessary for drawing conclusions, but instead we are relating sample surface structure to a pathway of water vapor condensation and ice growth.

### Specific comments

Page 1 line 16 Heterogeneous ice nucleation is not limited to temperatures above  $-36^{\circ}\text{C}$ . Deposition ice nucleation relevant for cirrus cloud formation occurs at lower temperatures and below water saturation. As the experimental setup described in this manuscript might become useful to investigate deposition ice nucleation, I recommend mentioning it here in the introduction.

We have included this point in the discussion and outlook, “The setup described here is also applicable to studying deposition mode nucleation at sub  $-36^{\circ}\text{C}$  and sub-saturation (relevant to cirrus cloud formation), and optical observations of immersion mode nucleation on substrates.”

Page 1 line 24 The parametrization by DeMott et al., 2010 is not based on size as an ice nucleation property, but simply relates the concentration of INP to the concentration of particles above a threshold size, not implying that only these particles act as INP. This is often misinterpreted, please revise.

We changed “based on macroscopic properties like aerosol size” to “relating the concentration of INPs to the concentration of particles above a threshold size”.

Page 1 line 26 Useful parametrizations should capture various situations. Please elaborate and provide references supporting the claim that the mentioned parametrizations are not accurate outside the conditions for which they were developed. Also, surface site density of ice active sites derived from field measurements and laboratory studies have been used to parameterize ice formation in models eg., Vergara-Temprado et al., 2017. This could be mentioned.

We changed this sentence to “However, as is true for extrapolations in general, such models are expected to be less accurate when applied to conditions outside the range of measured values used to fine tune these models,”, and included the reference to Vergara-Temprado et al.

Page 1 line 31 Please specify what kind of information microscopy can provide to distinguish mechanisms of ice nucleation.

By imaging the surface structure at an ice nucleation site, microscopy can provide additional information regarding condensation versus direct vapor deposition mechanisms if pores, cracks, or stepped structures are resolved or not. To further clarify this point we have modified the end of this sentence to read, “innovative microscopy aimed at uncovering the local structural and chemical properties of ice nucleation sites is needed.”.

Page 2 line 3f It is unclear how the 10nm size is derived. Given the resolution of light microscopy, pixel size etc., used in the current setup it seems unrealistic to detect such small objects, making the discussion of framerate and its dependence on temperature and humidity conditions irrelevant. What is the smallest detectable size in the current setup and what is the limiting component?

This part of the paper presents an introduction to the challenges faced by using high resolution microscopy to study ice nucleation events. It is not a discussion of our approach, or our results. The 10 nm size is an order-of-magnitude benchmark based on the discussion in the first paragraph relating to critical-nucleus size. The value is used to exemplify the scale which non-optical microscopy techniques must be able to resolve, and at high frame rates, to truly observe ice nucleation at a definitive site.

Page 2 line 15 Clarify how this estimate was made. The resolution is 1.6um? This seems not to be high enough to see growth of 1um crystals. In addition, I calculate at least 10-times longer growth needed to reach this size at this conditions. The mentioned growth rate indicates a  $RH \gg 100\%$  and questions the control of relative humidity in the experiment. Ice growth can be used to infer humidity in the specimen chamber (see S3 in Kiselev et al., 2016). I highly recommend a comparison of relative humidity based on ice growth rates and the method used by the authors to determine humidity.

We give an estimate of growth velocity for these structures, treating the projected area as an effective circle, only to serve as an example of the speeds involved in our observations of ice growth. Our growth rate is based on measurements made when the crystal is resolved optically (greater than 1um) then extrapolated to represent small length-scales. The growth habits we observe are polycrystalline, highly branched crystal clusters, whereas the velocity equation used by Kiselev et al., 2016 assumes an atomically flat spherical surface.

Page 2 line 16f Please elaborate how high-speed AFM can advance heterogeneous nucleation research.

HS-AFM can advance heterogeneous nucleation research by directly observing nucleating crystals with 10 nm resolution, or less, by way of high frame-rate AFM. This has the potential to yield the best nucleation site location accuracy of the techniques currently available. We added to the manuscript: "... if emerging ice crystals could be observed directly with ~10 nm resolution, thus improving significantly the accuracy of locating nucleation sites."

Page 2 line 20 How accurate can the site of ice formation be located with this setup? It is mentioned on page 2 line 1 that the spatial resolution must be on the order of nanometers to locate the ice nucleation site. Please derive the minimum resolved distance for your camera system and verify with a resolution target. A discussion of what accuracy would be desirable in contrast to what can be achieved would be helpful to clarify down to what scale the setup can be sensitive.

In our setup, we are ultimately limited by the wavelength of visible light used for optical microscopy. No light-based microscopy – including our own – would be sufficient to specify a nucleation site with any accuracy.

Page 2 line 22 Surface features on a feldspar specimen of the size used in this study might not be present on micrometre sized dust particles found at mixed-phase cloud level, and therefore be not relevant for ice nucleation on these particles. I recommend not to emphasize atmospheric relevance.

The morphological features we analyze in this paper are simple surface steps, which are ubiquitous and expected to be abundant on most if not all feldspar dust particles. However, the small size and the complex morphology of these aerosol particles makes it impossible to acquire high-resolution AFM data and isolate the role of individual surface steps. Also in response to reviewer #1, we added text to the manuscript intended to clarify the atmospheric relevance:

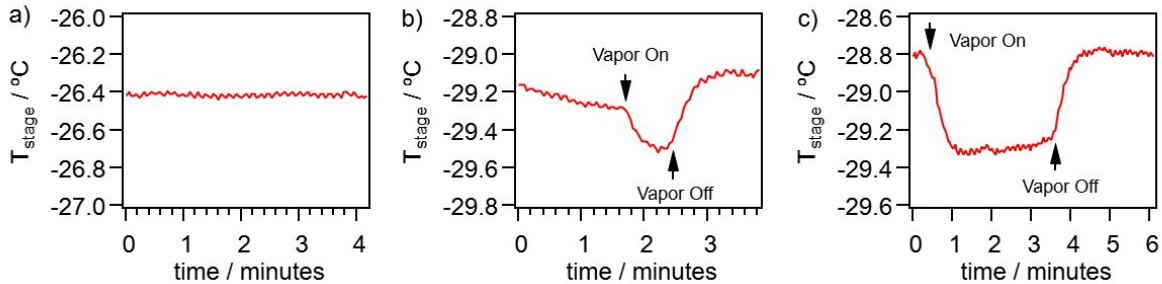
Before the last sentence of the introduction we added: *"While studying aerosol particles collected from the atmosphere would provide a more direct connection to atmospheric conditions. The typically complex structure and chemistry of these particles often precludes identifying the individual nanoscale processes that are important. For this study, instead, we choose extended flat substrates of known composition on which the role of individual topographic features can be examined."*

And to the discussion and outlook section we added: *"In the discussed example of ice formation, the step-height analysis is used to corroborate the involvement of the liquid phase of water during the observed rapid formation and propagation of ice on feldspar..."*

Page 3 line 1ff Provide a temperature calibration to demonstrate the stability (1°C/hr mentioned in Sec.2.2.), accuracy of temperature control and homogeneity in the mixing chamber. Temperature control is crucial to study ice nucleation and therefore the interpretation of observations made with the setup. Please clarify if temperature is actively controlled or only monitored with the TC-720. Active temperature control is desirable for this type of setup.

The temperature control in this work is passive and monitored by the TC-720 controller. Typical experiments last less than 60 seconds (vapor flow on-to-off time). While we agree that strict temperature control is important when quantifying nucleation kinetics, we are not engaging those experiments here. The 1°C/hr stability figure was regularly observed during setup of experiments,

however it was not recorded. In lieu of this data we show the stability of the stage temperature over the minutes timescale for three cases: a) without vapor flow, b) during a short vapor flow experiment, and c) a long vapor flow experiment. In section 2.2 we have revised the paper to remove the mention of 1°C/hr, and instead include a discussion regarding the temperature variation during an experiment, “During the course of an icing experiment the temperature measured at the sample stage decreases by approximately 0.5 °C due to the diverting of a portion of cold gas back to the stage when the vapor flow is turned on.”



Page 3 line 11 Ice and mixed-phase clouds form at a variety of conditions. Ice clouds do not require water saturated conditions. Specify conditions that can be created in the mixing chamber.

Because the final humidity in the chamber is a mixture of vapor and dry flows, in principle the full range of humidities below saturation can be explored by adjusting the relative flow rates.

Page 3 line 17f How is frost formation in the mixing column prevented?

Over repeated experiments we do eventually form ice in the small mixing column portion of the cell. The small size of the column leads it to become clogged quickly once ice forms. This then leads to no flow into the cell. We remedied this by clearing out the cell with warm dry nitrogen between experiments.

Page 3 line 20f Advantages compared to what other technique? What can be learned from using different flow rates?

Control over total flow rate is useful in practice for various reasons. Large flow velocities can disrupt growing ice crystals that may be weakly bound to a substrate. On the other hand, if one were limited to slow flow rates this would cause long delays when changing cell conditions from, for example, low humidity to a desired humidity. The flow rates one might require will be substrate-dependent and also will depend on the conditions one is attempting to create within the cell (e.g. turbulent, laminar, etc.).

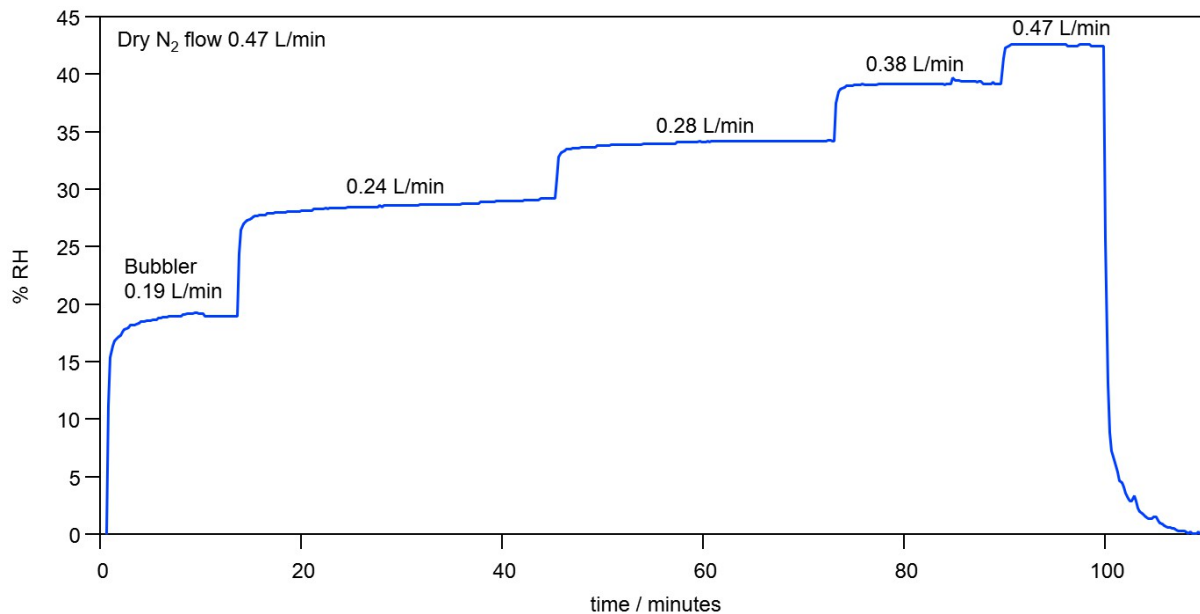
Page 3 line 23f Please explain why thermal gradients are minimized by that.

In a cold-stage only setup the gas above the sample is cooled by the stage. This results in a gradient in temperature from the gas-sample interface upwards. Here we have minimized this gradient by also flowing cold gas into the chamber so the sample is cooled from above and below. To make this clearer we modified this sentence to “*In our setup, a cold atmosphere flows into the small ~ 30  $\mu\text{L}$  volume cooling the sample from above and below, thus minimizing temperature differences laterally and from the sample-gas interface upwards.*”

Page 3 line 32 Please provide exemplary time series of temperature and relative humidity during an experiment. What is the purpose of switching the wet flow on and off? Could the humidity sensor be used to measure humidity in the outlet flow to verify the humidity in the chamber?

Page 4 line 1 How long does it take to reach steady-state humidity? To vary the humidity in the mixing chamber the flow through the bubbler is adjusted. Does this change steady state? Provide measured humidity after the bubbler as function of flow rate. Another strategy to adjust humidity in the wet flow might be to change the temperature of the bubbler.

The vapor flow is turned on and off to control the generation of ice during an experiment. We did not use the outlet to measure humidity because the humidity sensor time to steady state is long compared to the experiment. This is partly due to the capacitive sensor used for RH measurement as well as the volume around the sensor that must be exchanged. The humidity exiting the chamber over time is also convoluted by the ice growth within the small chamber volume, further compounding the inaccuracy of the final RH measurement. As an illustration, we include here the measured humidity at the outlet of the sample chamber at room temperature under similar conditions to typical experiments. Varying the flow rate of the bubbler changes the proportion of vapor mixed into the constant dry nitrogen flow. Changing the flow rate also changes the time with which steady state is reached. For example, in the data shown below, at the lowest bubbler flow rate the effective sensor time constant is approximately 45 seconds, while at the highest bubbler flow the time constant is about 20 seconds. These times are far too long for the typical duration of an icing experiment which is less than 1 minute.



Page 4 line 9ff Knowing and controlling the relative humidity (RH) in the experiment is essential for interpretation of results and to infer the ice nucleation mechanism. Calibration of relative humidity should be done much more carefully by eg., using a dew point mirror to measure humidity in the outflow of the chamber. While AH might be useful to determine flow rates of the wet flow, chamber conditions should be reported as relative humidity and temperature. Convert AH to RH throughout the manuscript.

We opted to provide the estimated AH input to the cell rather than a RH because the RH is unknown at the surface location where we observe the ice formation/growth. Since we are not calculating quantitative kinetic parameters related to ice nucleation we show here the trend for increasing humidity without declaring that we have accurate knowledge of the actual humidity where the events take place.

Page 4 line 19 Converting the error in AHin of 0.08g/m<sup>3</sup> to RH gives +/- 18% which is a very high uncertainty for ice nucleation experiments.

Please see above.

Page 5 line 1 AHin reported here and considering the uncertainty given on the last page, relative humidity is equal to RHw= 85% +/- 18%. Conditions above water saturation are within the experimental accuracy, making the interpretation of the data as purely deposition ice nucleation imprecise. This underlines the point made in the comment above, that control of the experimental conditions is insufficient for ice nucleation experiments. Compare estimated saturation conditions against calculation based on ice crystal growth rate or measure the humidity at the chamber outlet.

Please see above.

Page 5 line 3 Couldn't AFM detect pores on the substrate? What is the horizontal resolution of AFM used here?

The AFM can routinely detect features down to sub-10 nm in size. However, the optical and temporal resolution of our camera is not adequate to observe an ice nucleation event – it can only record the subsequent growth of the ice crystals. Therefore, any attempt to associate a point on an AFM image with an ice crystal's nucleation site will have an error of several microns.

Page 5 line 5 "Ice formation" instead of "ice nucleation" would be more accurate.

We agree with the referee and we have changed this in the text.

Page 5 line 12ff What is discussed here is ice growth and not ice nucleation. Inferring ice nucleation mode from this observation seems over-reaching. The two processes (ice growth and ice nucleation) should be separated more clearly throughout the manuscript.

We agree and have changed this from "mode" to "pathway".

Page 6 line 14 All four humidities applied are high above water saturation (RH=134%, 167%, 201%, 234%). It is surprising to see sensitivity of ice formation on the amount of supersaturation in this high humidity regime other than a change in growth rate. As pointed out in the discussion, different growth rates are a more plausible explanation for the observation than the probability of ice nucleation. The context in which the experimental results are interpreted should be clarified. Is it about ice growth or ice nucleation mechanisms?

The RH at the surface is clearly not given by the numbers mentioned above, otherwise the cell would be full of water. This is why we provide the input AH to convey the trend in humidity without claiming precise knowledge of the actual humidity at the surface. The benefit of using humidity greater than

saturation is that it reveals very clearly the ability of surface steps to provide pore-like condensation channels. If we limited our experiments to RH at saturation, the limited water content in the channels would be quickly dehydrated once ice is formed nearby, making it difficult to observe the ubiquitous nature of the water channels on the surface. The larger context of our results is that by combining surface topography with optical microscopy we can better define the pathway to ice formation on surfaces.

Page 7 line 5 Please provide the resolution of the current setup. Is the CCD pixel size limiting the resolution?

We are limited to about 1.6  $\mu\text{m}$  resolution, which is partly a function of the NA of our long-working distance objective. We are not limited by the CCD pixel density.

Page 10 Fig.2 check if there is a mix-up between e), d). The description in the figure caption seems to be switched. Images show a scale bar of 5 $\mu\text{m}$  and this seems to be a typical scale how accurate ice formation can be located. In the introduction it is correctly mentioned that ice nucleation occurs on structures with a scale of few nanometres. Features in eg. e) are on a 1000-times larger scale, questioning the interpretation as ice nucleating sites.

The scale bars here are correct. We modified the caption to “... (e) Expanded view of a portion of panel (d)...”. We did not intend to claim that we are able to pinpoint ice nucleation sites. We circle the area within which nucleation occurs and subsequently and ice crystal emerges. We do not claim to have isolated the precise site.

Page 10 Fig. 3 replace AH with RH (=167% +/- 18%).

Page 12 Fig. 6 b) replace AH with RH (=134%, 167%, 201%, 234% +/-18%) .

Please note the discussion above. We are currently unable to precisely define the RH at the surface and throughout the experiment, and therefore have opted to provide the approximate AHin for each run.

### References

- DeMott, P. J., Prenni, A. J., Liu, X., Kreidenweis, S. M., Petters, M. D., Twohy, C. H., Richardson, M. S., Eidhammer, T., and Rogers, D. C.: Predicting global atmospheric ice nuclei distributions and their impacts on climate, *Proceedings of the National Academy of Sciences*, 107, 11 217–11 222, <https://doi.org/10.1073/pnas.0910818107>, 2010.
- Kiselev, A., Bachmann, F., Pedevilla, P., Cox, S. J., Michaelides, A., Gerthsen, D., and Leisner, T.: Active sites in heterogeneous ice nucleation—the example of K-rich feldspars, *Science*, 355, 367–371, <https://doi.org/10.1126/science.aai8034>, 2016.
- Vergara-Temprado, J., Murray, B. J., Wilson, T. W., O'Sullivan, D., Browse, J., Pringle, K. J., Ardon-Dryer, K., Bertram, A. K., Burrows, S. M., Ceburnis, D., DeMott, P. J., Mason, R. H., O'Dowd, C. D., Rinaldi, M., and Carslaw, K. S.: Contribution of feldspar and marine organic aerosols to global ice nucleating particle concentrations, *Atmos. Chem. Phys.*, 17, 3637–3658, <https://doi.org/10.5194/acp-17-3637-2017>, 2017.

# Mapping ice formation to mineral-surface topography using a micro mixing chamber with video and atomic-force microscopy

Raymond W. Friddle<sup>1</sup> and Konrad Thürmer<sup>1</sup>

<sup>1</sup>Sandia National Laboratory, Livermore, 94550, USA

5 *Correspondence to:* Raymond W. Friddle ([rwfridd@sandia.gov](mailto:rwfridd@sandia.gov)), Konrad Thürmer ([kthurme@sandia.gov](mailto:kthurme@sandia.gov))

**Abstract.** We developed a method for examining ice formation on solid ~~materials under~~substrates exposed to cloud-like ~~conditions at~~atmospheres. Our experimental approach couples video-rate optical microscopy of ice formation with high-resolution atomic force microscopy (AFM) of the initial mineral surface. We demonstrate how colocating stitched AFM images with video microscopy can be used to relate the likelihood of ice formation to nanoscale properties of a mineral substrate, e.g., the abundance of surface steps of a certain height. We also discuss the potential of this setup for future iterative investigations of the properties of ice nucleation sites on materials.

## 1 Introduction

Ice formation in the atmosphere initiates most precipitation and strongly affects Earth's radiation balance (Pruppacher and Klett 1997; Rogers and Yau 1989; Lohmann and Feichter 2005; DeMott et al. 2010; Lau and Wu 2003). Ice emerges via various microscopic processes (Kanji et al. 2017; Pruppacher and Klett 1997; Rogers and Yau 1989; Vali et al. 2015); some require the presence of a foreign material (heterogeneous nucleation) while others proceed unaided by any foreign substance (homogeneous nucleation). For ice nucleation to occur above  $\approx -36^\circ\text{C}$ , a suitable ice nucleating particle (INP) must provide a surface onto which an ice nucleus can grow to a critical size without being impeded by an insurmountable activation barrier. Most ice nucleation events occur at atmospheric conditions where the critical-nucleus size ranges from  $\sim 1$  nm to  $\sim 50$  nm (Pruppacher and Klett 1997). Uncovering the mechanisms involved in these events thus requires nanometer-resolution techniques.

While structure, morphology, particle size, and the presence of defects or functional groups have been found to determine the ice-nucleating ability of aerosols, the role of these properties and how they interact remains poorly understood (Coluzza et al. 2017; DeMott et al. 2011; Kanji et al. 2017; Koop and Mahowald 2013; Pruppacher and Klett 1997; Welti et al. 2014). Nevertheless, recent ice-nucleation parameterizations, ~~based on macroscopic properties like~~relating the concentration of INPs to the concentration of aerosol particles above a threshold size (DeMott et al. 2010), the aerosols' chemical composition (Vergara-Temprado et al. 2018), or water/substrate contact angles (Wang et al. 2014) and averaged field measurements, have succeeded in improving the accuracy of global climate models. However, as is true for extrapolations in general, such models are ~~not~~ expected to be less accurate when applied to conditions outside the range of measured values used to fine tune these models, e.g., to predict a changing environment due to global warming or to predict the behavior under extreme regional conditions, say, in plumes of dust or contamination. Developing a capability to predict ice formation at these uncharted atmospheric conditions with some confidence will require a quantitative understanding of the underlying mechanisms. Since macroscopic measurements of nucleation rates often cannot distinguish clearly between nucleation mechanisms (Kanji et al. 2017; Marcolli 2014; Pruppacher and Klett 1997; Welti et al. 2014; Vali et al. 2015), innovative microscopy aimed at uncovering ~~these mechanisms~~the local structural and chemical properties of ice nucleation sites is needed.

The technical requirements to adequately resolve ice nucleation in time and space are indeed demanding. The imaging system must operate in humid environments, at sub-0 °C temperatures, be non-destructive, and offer spatial resolution on the order of nanometers. Finally, to locate the ice nucleation site to within nanometers, the frame rate must be fast enough to capture the earliest emergence of the crystalline phase. As a point of reference, our data at  $\approx -30$  °C and relative humidity RH  $\approx 100$  % suggest that capturing just one frame of a new ice crystal smaller than 10 nm would require imaging at rates greater than 1 Mfps ( $< 1$   $\mu$ s per image). This minimum frame rate decreases with lower temperature and humidity. Various groups recently demonstrated the resolving power of environmental scanning electron microscopy (ESEM) for studying ice nucleation (Kiselev et al. 2016; Wang et al. 2016; Zimmermann et al. 2008). Unfortunately, ESEM is unable to operate under realistic atmospheric pressures and is prone to introducing electron-beam damage and local heating of condensed water (Rykaczewski, Henry, and Fedorov 2009).

AFM is unique among high-resolution microscopies in that it non-destructively generates the 3-dimensional topography of a surface. Furthermore, the force-based imaging principle of AFM permits it to operate in a broad range of environmental conditions, including exposure to gases, liquids, and varied temperatures. This environmental versatility would appear to make AFM well-suited for *in situ* imaging of cloud-like icing processes on the surface of particulates or other samples. However, a key limitation of most commercial AFMs is their slow imaging speed. A typical AFM scan of sub-micron size can take between 10 seconds to 10 minutes depending on flatness of the substrate, the field of view (FOV), and the desired resolution. Meanwhile at RH  $\approx 100$  % and  $\approx -30$  °C we estimate that a new ice crystal reaches an effective diameter of 1  $\mu$ m in just 6 ms<sup>1</sup>. Current developments in high-speed AFM (HS-AFM) are encouraging, ~~however (Ando 2014; Russell-Pavier et al. 2018),~~ and have the potential to significantly advance heterogenous nucleation research (Ando 2014; Russell-Pavier et al. 2018), if emerging ice crystals could be observed directly with ~10 nm resolution, thus improving significantly the accuracy of locating nucleation sites.

By combining the speed of optical microscopy with the spatial resolution of AFM, the limitations of the individual instruments can be mitigated by colocation. Here we present an approach to connect optical images of ice forming locations to AFM data that resolve mineral substrate surface structures at the nanometer scale. While studying aerosol particles collected from the atmosphere would provide a more direct connection to atmospheric conditions. The typically complex structure and chemistry of these particles often precludes identifying the individual nanoscale processes that are important. For this study, instead, we choose extended flat substrates of known composition on which the role of individual topographic features can be examined. We demonstrate our approach on a substrate of K-feldspar (orthoclase), where we observe and quantify how surface steps facilitate ice formation—a phenomenon pertinent to ice nucleation and growth in mixed-phase clouds.

## 2 Experimental apparatus and methods

### 2.1 Setup of a small mixing chamber AFM with video microscopy

#### 2.1.1 Overview of AFM, video, and gas flow components

The experimental setup (Figure 1) is built around a Multimode 8 AFM operated by a Nanoscope V controller (Bruker, Santa Barbara, CA). The AFM is seated on a Nikon top-down microscopy stage equipped with a 10X long-working-distance lens (WD

---

<sup>1</sup> Based on video observations of projected areal growth rate of an ice crystal of 130  $\mu$ m<sup>2</sup>/s treated effectively as a circle.

= 49.5mm, NA = 0.2, resolution approximately 1.6  $\mu\text{m}$ ). Video microscopy is recorded with an Infinity3-3URC 2.8 MP, 53 fps, color CCD camera. The AFM scanner, head, and objective lens are maintained in a dry nitrogen environment by a cylindrical acrylic atmospheric hood (MMAH2, Bruker). Thermally conductive epoxy (KONA 870FT LVDP, Henkel) is used to adhere the sample to a glass slide which is glued to a copper standoff stage. The standoff stage creates open space between the sample and the AFM piezo for underside cooling and placement of a thermistor.

Cold nitrogen gas is used for cooling both the substrate and the gas above the substrate. Ultrapure nitrogen gas, initially at room temperature, flows through a heat exchanging copper coil immersed in a dewar of liquid nitrogen. The final temperature of the cooled nitrogen is controlled by mixing with room temperature nitrogen. The cooled nitrogen is then divided into two paths: one cools the underside of the copper standoff stage, the other enters an inlet of the AFM sample cell. Water vapor is generated by flowing ultrapure dry nitrogen through a water bubbler. The humidity of the resulting room-temperature vapor is measured using a humidity sensor (ThermaData Series II – HTF, ThermoWorks). This vapor is then piped directly into the second inlet of the AFM sample cell. The temperature of the sample cell is monitored by thermistors placed at the underside of the copper standoff and the outlet of the sample cell. The thermistor readings are recorded in real time using a TC-720 thermoelectric temperature controller (TE Technology, Inc.).

### 2.1.12 Micro Mixing Chamber

To create a cloud-like ~~conditionsatmosphere~~ in a small-volume sample chamber requires humidity near saturation ( $\text{RH} \approx 100\%$ ) at sub-zero temperatures ( $< 0\text{ }^\circ\text{C}$ ). This is difficult to achieve in practice since delivering water vapor through a small tube at freezing temperatures will inevitably clog the tube with ice. Therefore, the vapor must remain above freezing temperatures during transport to the sample cell, then immediately cooled to the desired temperature. To achieve this combination of cold and humid gases we use a glass AFM fluid cell with three ports (Bruker, model ECFC): two ports located next to each other deliver the gases which combine upon entry into the sample chamber, while the third port serves as an outlet. The port arrangement is shown in Figure 1a. This configuration separates the sub-zero dry nitrogen from the water vapor until reaching a small mixing column at the entry into the sample chamber. The volume of the sample chamber is approximately 30  $\mu\text{L}$ , enabling rapid exchange of gases.

A number of advantages come with the mixing-chamber approach to observing ice formation. Since the entry gas is already at the desired temperature, a range of flow rates can be explored, without concern for cooling by interaction with a cold surface. In a cold stage approach, measures must be taken to ensure that the coldest part of the cell volume is the sample under study (Wang et al. 2016), otherwise water will condense on unwanted components. By flowing In our setup, a cold atmosphere flows into the small  $\sim 30\text{ }\mu\text{L}$  volume, ~~thermal gradients are minimized~~ cooling the sample from above and below, thus minimizing temperature differences laterally and from the sample-gas interface upwards. The last point has the additionalpotential benefit of keeping the AFM tip near the same temperature as the sample surface, ~~offering the potential~~ allowing, in principle, to image ice or the sample surface without raising their temperature (not explored here).

### 2.2 Experimental procedure

First, we pre-record detailed maps of the mineral-surface morphology with AFM at room temperature using a Tap150Al-G probe (Budget Sensors) without introducing humidity. To be able to capture a relatively large surface area of typically  $\sim 750 \times 570\text{ }\mu\text{m}^2$  while maintaining sub-nanometer height resolution, we developed an AFM stitching procedure described in Section 2.3. Subsequently, we performed ice growth experiments by exposing the same mineral surface region to a cold and humid environment

at atmospheric pressure. Here, we optically monitor the icing process at constant temperature while switching on and off the flow of water vapor. Following the diagram in Figure 1, a single source of compressed nitrogen supports three primary gas pathways: the humidifying bubbler, the warm mixing line, and the LN<sub>2</sub> cooling dewar. The sample temperature is set by adjusting the mixing ratio of room-temperature nitrogen to LN<sub>2</sub>-cooled nitrogen until the sample thermistor reads the desired temperature. ~~After settling for approximately 1 hour, we found~~ During the course of an icing experiment the temperature measured at the sample stage decreases by approximately 0.5 °C due to ~~be stable within 1°C/4hr~~ the diverting of a portion of cold gas back to the stage when the vapor flow is turned on. Most of this cold dry nitrogen stream is delivered to the base of the sample holder, while a small fraction is directed to one of the sample cell inlets. During temperature settling, a 3-way diverting valve passes the humidified nitrogen gas exiting the bubbler through a humidity sensor to measure its relative humidity. This maintains a dry, cold sample chamber while the vapor stream reaches a steady-state humidity. To inject water vapor into the cell, the 3-way valve above the bubbler is switched to divert the vapor stream into one of the mixing inlets of the cell. The vapor mixes with the steady stream of cold gas to supply cold vapor to the sample chamber. To halt the experiment, the vapor is again diverted to the humidity sensor. The ice is then removed from the surface before the next experiment through sublimation under dry N<sub>2</sub> and increasing the temperature above 0 °C.

Absolute humidity values (AH<sub>in</sub>) provided hereafter represent estimates of the water content of the gas stream injected into the environmental chamber. Note that after condensation and especially ice formation has started, the atmosphere in the microliter environmental chamber enters a non-equilibrium stage, in which the local humidity, especially near growing ice features, can be much lower than the given AH<sub>in</sub> values. We estimate AH<sub>in</sub> by calibrating against the saturation (RH ≈ 100 %) condition. That is, we find the lowest vapor flow rate which results in the onset of condensation on the feldspar surface. We then calculate the absolute humidity at T = ~~-30~~29.5 °C and RH = 100 % to find AH<sub>100</sub> = 0.4548 g/m<sup>3</sup> at a flow rate of Q<sub>100</sub> = 0.28 L/min, where AH<sub>100</sub> and Q<sub>100</sub> represent the absolute humidity and flow rate *at saturation* for that temperature. For constant dry cold flow rate, we assume the fraction of humid gas incorporated into the total inlet gas to be linear over the flow rates employed here (0.28 – 0.66 L/min). Therefore, for a humid line flow rate, Q, the humidity injected into the cell is approximated by,

$$AH_{in} = AH_{100} \frac{Q}{Q_{100}}.$$

We estimate that a 0.05 L/min error exists in our measurement of flow rate leading to an error for AH<sub>in</sub> of ±0.08 g/m<sup>3</sup>.

### 2.3 AFM image stitching

Several AFM images covering a relatively large area of the feldspar surface were acquired on a Dimension 3100 (Bruker), with a Nanoscope V controller, in tapping mode. This AFM has a motorized XY stage that allows programming a grid of images to be acquired at locations that cover the desired surface region. A mosaic is produced by stitching together a 6x9 array of 54 individual AFM images, each with a 100 × 100 μm<sup>2</sup> scan size and typical overlap of 10 μm with neighboring images. The large scan size and acquisition time result in appreciable background warping of the individual images. To optimize stitching of adjacent images with minimal seam lines requires flattening each image. In most cases we subtracted a 2D polynomial of first order in *x* and second order in *y*,  $\sum_{j=0}^1 \sum_{k=0}^2 a_{j,k} x^j y^k$ , which is fitted to masked areas of constant height. The resulting image is then levelled by an iterative routine which optimizes levelling of surface facets (software: Gwyddion). Image borders are seamed by alpha blending such that the image height, *h<sub>i</sub>*, across the overlap of images *i* = 1,2 is blended by  $h_{tot} = \alpha h_1 + (1 - \alpha) h_2$ , where *α* varies linearly

from 0 to 1 across the width of the overlap. Note that quantitative analysis of step heights is performed on the original individual images to avoid errors caused by seams. Image alignment and blending is performed using a custom routine in Igor Pro (Wavemetrics).

### 3 Experimental results

5 We used the system described here to examine ice formation on a sample mechanically cut from single crystal K-feldspar along the (001) easy-cleavage plane (Orthoclase,  $\text{KAlSi}_3\text{O}_8$ , Yavapai County, Arizona, USA, vendor: VWR/Eric Miller). In this study we maintain a fixed temperature of approximately  $-3029.5 \pm 0.5$  °C while recording video of ice formation at different humidities. At humidity below saturation ( $\text{AH}_{\text{in}} = 0.3840 \pm 0.08$  g/m<sup>3</sup>), we find growth of isolated ice crystals on the feldspar surface with no precursor condensation of liquid water resolved optically (Fig. 2a-c). While this is consistent with a direct vapor deposition nucleation mechanism we are unable to rule out capillary condensation at sub-micron length-scales within confined surface structures- (Christenson 2013; David et al. 2019; Fukuta 1966; Marcolli 2014; Pach and Verdaguer 2019). Near saturation with respect to water ( $\text{RH} \approx 100\%$ ,  $\text{AH}_{\text{in}} = 0.4548 \pm 0.08$  g/m<sup>3</sup>), we observe condensation of water droplets on the K-feldspar surface (Fig. 2f-h). Ice nucleation formation at various sites occurs either concomitantly with condensation or after a short induction period. Alongside the optical images of ice formation in Fig. 2 are AFM images of the same locations. We find that many distinct surface sites repeatedly nucleate ice across multiple experiments, and over varied humidities, which agrees with ESEM findings of active sites on orthoclase for heterogeneous ice nucleation (Kiselev et al. 2016). However, we also observed that after covering the surface with liquid water, then subsequently drying the surface before repeating an ice experiment, some sites lost their ice nucleating ability while previously inactive locations became sites for nucleation.

10

15

20 Above saturation, we observe a very different ~~mode-of-pathway to~~ ice formation. As shown in Fig. 3, the initially dry surface is first darkened by the condensation of water droplets on the sample surface. Shortly thereafter, rough filaments of ice branch out across the surface. A denuded zone is established as a halo absent of water droplets around these ice filaments. After the elongation of the filaments halts, the width of the ice filaments continues to grow as water from the surrounding vapor attaches to the crystals. Qualitatively comparing the optical images to the collocated AFM image in Figure 3, it appears that the ice filaments follow the contour of surface step edges. In Figure 4 we show that this is indeed the case. There, a frame of optical data taken when the ice filament extensions have ceased (Fig. 4b), is overlaid on a mosaic AFM image of the same area (Fig. 4a) to produce a collocated composite (Fig. 4c). Clearly, the ice decorates many of the prominent step edges on the surface. The emergence of these ice-filament patterns has been described in more detail in (Friddle and Thürmer 2019a). We also find a few isolated ice crystals (two are labelled in Fig. 4b), which despite having been surrounded by nearby droplets supplying water, did not merge with the main continuous system of ice filaments. Comparing the surface structures underlying these isolated crystals to that for filaments in Figs. 4d-g, we see that for the surfaces where ice forms extended filaments the surface presents tall step edges that run uninterrupted along the extension of the ice filament's path (Figs. 4f,g). The substrate surfaces underlying the isolated ice crystals, on the contrary, display island-like protrusions spanning relatively short distances (Figs. 4d,e). Our data neither reveal nor rule out any preferred crystal orientation of the observed ice structures.

25

30

## 4 Data processing

### 4.1 Analysis of surface steps

Figure 5 illustrates the process we developed to extract step heights from the AFM data and relate those to the optically-observed ice-forming locations. An AFM image (Fig. 5a) is first converted to an image of step-heights (Fig. 5b), where traces outline where the step edges lie, and the value of each pixel along the trace corresponds to the step's height at that point. This step-edge image is generated by the following custom routine (Igor Pro, Wavemetrics) operating on the row and column 1D arrays of the 2D image matrix: After background subtraction, the derivative of the 1D array is taken. An edge is found when the rate-of-change of the differentiated array crosses a threshold of  $d^2z/dx^2 = 6 \text{ nm/mm}^2$ , which detects step heights greater than 2 nm. Once a crossing is found, the local peak and two floor points of the derivative array are used to determine the step height from the original array. The step edge location and height are assigned to a pixel on the new image. This process is repeated, line-by-line, along the rows and columns of the AFM image.

The step edge image is interactive (Fig. 5b) to facilitate manually collecting step-height statistics over many step segments. Contiguous pixels of similar step height are grouped into clickable trace segments which change color and thickness to indicate selection (see Fig. 5d). Selection is reversible, and trace segments can be cut into smaller segments where needed to match the iced segment lengths observed optically.

#### 4.1.2 Relating ice formation to step heights

Once registration between the AFM step height image and optical image is established, the routine discussed in section 4.1 is applied to collect statistics on the heights of step edges along which ice forms. As shown in Figure 5, the selected step edges in panel 5d are chosen to coincide with the filaments of ice in panel 5c. The selected trace segments contain step height values for each pixel along the segment. This is repeated for all the images across the desired analysis area. The selected step heights are binned into a histogram and compared against a histogram of all step heights presented in the image. Binning is counted as pixels or physical length.

Figure 6 shows an example of processed step height data collected over 15 images, each covering  $100 \times 100 \mu\text{m}^2$ . Here we show histograms for ice formation on K-feldspar at four different humidities, all at a temperature of  $-3029.5 \pm 0.5 \text{ }^\circ\text{C}$ . Each histogram is derived from one video frame for each humidity which is chosen based on when ice propagation across the surface has halted. Figure 6 shows the distribution of step heights for a) all steps observed and b) steps on which ice propagates. The ratio of these two histograms – total length of iced steps within a step-height bin over total length of *all* steps (within the same step-height bin) – provides the probability of finding ice on a step of a given height (Fig. 6c).

## 5 Discussion and outlook

The data in Figure 6c reveals that, above saturation, ice is more likely to form along taller steps than shorter steps. Furthermore, the sigmoidal probability distribution in Fig. 6c shifts with changing humidity: as the humidity is increased, the curve moves towards smaller step heights. As detailed in (Friddle and Thürmer 2019a), the formation of ice filaments along step edges can be explained by capillary water condensation, with water filling the bottom corner where the step edge meets the underlying terrace. The orthoclase water contact angle is  $\sim 45^\circ$  (Karagüzel et al. 2005), and in principle, above thus, at saturation, perpendicular steps of all heights will be lined with water wedges when the surface's water contact angle  $\leq 45^\circ$  (Brinkmann and Blossey 2004; Moosavi,

Rauscher, and Dietrich 2006; Seemann et al. 2011). Therefore, steps of any height are pre-filled with liquid water which can freeze in place once a nucleation event occurs anywhere along the step. However, a step height-dependence of ice formation. This process can be viewed as an extension of the pore condensation and freezing mechanism (Christenson 2013; David et al. 2019; Fukuta 1966; Marcolli 2014; Pach and Verdaguer 2019) to higher humidity. A step height-dependence of ice growth arises from the subsequent dehydration of water wedges as denuded zones form around existing ice crystals. The taller steps contain more water, and thus can retain water wedges longer than their shorter neighbours. Hence the transformation of water wedges to ice, due to heterogeneous nucleation or contact with a nearby ice filament, has a greater window in time to occur with taller steps. This capillary-based mechanism is consistent with the ice formation shown in Figure 4. Here, ice filaments grow when step edges maintained tall heights for extended distances, whereas isolated ice crystals were observed at protrusions or depressions surrounded by flat areas.

Typically, most aerosol particles are completely immersed in a cloud droplet already at very modest supersaturations. As discussed in detail in (Friddle and Thürmer 2019a), the step-facilitated mechanism described above is expected to be relevant when a cavity-free feldspar particle, initially devoid of ice, is suspended in air colder than  $-20^{\circ}\text{C}$  that becomes slowly saturated. According to Fletcher's estimate (Fletcher 1962; Pruppacher and Klett 1997) that a humidity of  $\text{RH}_w > 130\%$  is required for a measurable nucleation rate of water droplets with a contact angle of  $\approx 45^{\circ}$  on a planar insoluble substrate. Hence condensation of supercooled water will be confined to step edges, where the water will freeze rapidly, thus initiating ice formation.

In the discussed example of ice formation, the step-height analysis is used to corroborate the involvement of the liquid phase of water during the observed rapid formation and propagation of ice on feldspar, while the link between surface-step height and the ability of an isolated aerosol particle to initiate ice nucleation is neither direct nor obvious. Nevertheless, such step-height analysis might benefit future studies in fields of material science, like corrosion and aircraft icing (Gent, Dart, and Cansdale 2000; Kreder et al. 2016), where the behaviour of the examined materials is affected by the abundance of surface steps.

In the current implementation of the AFM/optical technique presented in this paper, the two microscopies are performed sequentially on the same surface area, and the data are subsequently merged for quantitative analysis of surface structure as it pertains to ice formation. Future experiments will explore simultaneous operation of AFM and optical microscopy, which may improve spatial localization of ice nucleation sites and resolving their morphologies. The setup described here is also applicable to studying deposition mode nucleation at sub  $-36^{\circ}\text{C}$  and sub-saturation (relevant to cirrus cloud formation), and optical observations of immersion mode nucleation on substrates. As previously demonstrated (Yang et al. 2015; Gurganus, Kostinski, and Shaw 2011; Yang et al. 2018; Holden et al. 2019), higher frame rates than used here are imperative when the sample is immersed in water because the ice can spread to millimetre length-scales on the order of milliseconds after the nucleation event. Nevertheless, higher video frame rates do not improve the resolving power of the microscope which is fundamentally restricted by the diffraction limit  $\sim \lambda/2\text{NA}$ . In our system the small numerical aperture of our objective ( $\text{NA} = 0.2$ ) follows from the large working distance lens required to fit within the clearance of the AFM. Dedicated microscopy systems can improve resolution by using higher NA and by implementing blue filters to limit the wavelength  $\lambda$ . Ultimately, advanced high-speed AFM may be the key to direct observations of ice nucleation events, as it has proven capable of performing high-speed imaging of dynamic processes at nanometer resolution under various environments (Yamashita et al. 2009; Payton, Picco, and Scott 2016; Pyne et al. 2009; Picco et al. 2008; Kodera et al. 2010; Uchihashi et al. 2011; Casuso et al. 2010).

40

Finally, the rapid spreading of ice we observed on feldspar, is expected to play a role in other circumstances where extended surfaces, covered with continuous networks of steps or grooves, are exposed to a supersaturated atmosphere, providing a microscopy-based argument for avoiding rough surfaces with large steps or grooves in efforts to prevent aircraft icing (Gent, Dart, and Cansdale 2000; Kreder et al. 2016).

5

*Video supplement.* Videos corresponding to the optical frames presented in figures 2a, 2b, 3a, and 4b can be found online at <https://doi.org/10.7910/DVN/DZUZ6P>.

10 *Data availability.* Raw AFM and optical video data supporting the findings of this study are available from RWF ([rwfridd@sandia.gov](mailto:rwfridd@sandia.gov)) or KT ([kthurme@sandia.gov](mailto:kthurme@sandia.gov)) on request.

*Author contributions.* RWF and KT conceived of and performed the experiments, analysed the data, and wrote the paper.

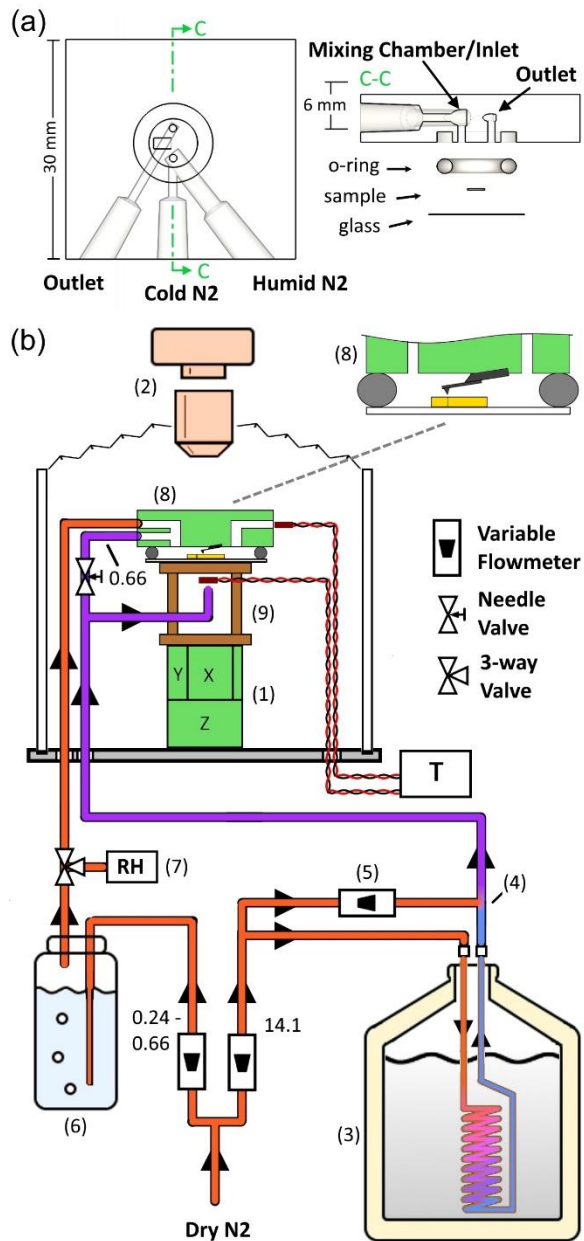
15 *Competing interests.* The authors declare that they have no conflict of interest.

*Acknowledgments.* We thank Norman C. Bartelt for insightful discussions. This work was supported by the Sandia Laboratory Directed Research and Development Program. Sandia National Laboratories is a multi-mission laboratory managed and operated by National Technology and Engineering Solutions of Sandia LLC, a wholly owned subsidiary of Honeywell International Inc. for the U.S. Department of Energy's National Nuclear Security Administration under contract DE-NA0003525.

## References

- Ando, T. 'High-speed AFM imaging', *Curr. Opin. Struc. Biol.*, 28: 63-68. 2014.
- 25 Brinkmann, M., and R. Blossey. 'Blobs, channels and "cigars": Morphologies of liquids at a step', *Eur. Phys. J. E*, 14: 79-89. 2004.
- Casuso, I., P. Sens, F. Rico, and S. Scheuring. 'Experimental Evidence for Membrane-Mediated Protein-Protein Interaction', *Biophys. J.*, 99: L47-L49. 2010.
- [Christenson, H. K. 'Two-step crystal nucleation via capillary condensation'. \*CrystEngComm\*, 15: 2030-39. 2013.](#)
- 30 Coluzza, I., J. Creamean, M. J. Rossi, H. Wex, P. A. Alpert, V. Bianco, Y. Boose, C. Dellago, L. Felgitsch, J. Frohlich-Nowoisky, H. Herrmann, S. Jungblut, Z. A. Kanji, G. Menzl, B. Moffett, C. Moritz, A. Mutzel, U. Poschl, M. Schauerl, J. Scheel, E. Stopelli, F. Stratmann, H. Grothe, and D. G. Schmale. 'Perspectives on the Future of Ice Nucleation Research: Research Needs and Unanswered Questions Identified from Two International Workshops', *Atmosphere*, 8: 28. 2017.
- [David, R. O., C. Marcolli, J. Fahrni, Y. Q. Qiu, Y. A. P. Sirkin, V. Molinero, F. Mahrt, D. Bruhwiler, U. Lohmann, and Z. A. Kanji. 'Pore condensation and freezing is responsible for ice formation below water saturation for porous particles'. \*Proc. Natl. Acad. Sci. U. S. A.\*, 116: 8184-89. 2019.](#)
- 35 DeMott, P. J., O. Mohler, O. Stetzer, G. Vali, Z. Levin, M. D. Petters, M. Murakami, T. Leisner, U. Bundke, H. Klein, Z. A. Kanji, R. Cotton, H. Jones, S. Benz, M. Brinkmann, D. Rzesanke, H. Saathoff, M. Nicolet, A. Saito, B. Nillius, H. Bingemer, J. Abbatt, K. Ardon, E. Ganor, D. G. Georgakopoulos, and C. Saunders. 'Resurgence in ice nuclei measurement research', *Bull. Am. Meteorol. Soc.*, 92: 1623-35. 2011.
- 40 DeMott, P. J., A. J. Prenni, X. Liu, S. M. Kreidenweis, M. D. Petters, C. H. Twohy, M. S. Richardson, T. Eidhammer, and D. C. Rogers. 'Predicting global atmospheric ice nuclei distributions and their impacts on climate', *Proc. Natl. Acad. Sci. U. S. A.*, 107: 11217-22. 2010.
- [Fletcher, N. H. \*The physics of rainclouds\* \(Cambridge University Press: New York\). 1962.](#)
- Friddle, R. W., and K. Thürmer. 'Direct observation of morphology-enhanced condensation and freezing on feldspar: How nanoscale surface steps promote ice formation', Manuscript submitted for publication. 2019a.
- 45 Friddle, Raymond, and Konrad Thürmer. 'Video microscopy of ice nucleation and growth on the (001) face of orthoclase at -30 C', Harvard Dataverse, <https://doi.org/10.7910/DVN/DZUZ6P>. 2019b.

- Fukuta, N. 'Activation of atmospheric particles as ice nuclei in cold and dry air', *J. Atmos. Sci.*, 23: 741-50. 1966.
- Gent, R. W., N. P. Dart, and J. T. Cansdale. 'Aircraft icing', *Philos. Trans. R. Soc. Lond. Ser. A-Math. Phys. Eng. Sci.*, 358: 2873-911. 2000.
- 5 Gurganus, C., A. B. Kostinski, and R. A. Shaw. 'Fast Imaging of Freezing Drops: No Preference for Nucleation at the Contact Line', *J. Phys. Chem. Lett.*, 2: 1449-54. 2011.
- Holden, M. A., T. F. Whale, M. D. Tarn, D. O'Sullivan, R. D. Walshaw, B. J. Murray, F. C. Meldrum, and H. K. Christenson. 'High-speed imaging of ice nucleation in water proves the existence of active sites', *Sci. Adv.*, 5. 2019.
- Kanji, Zamin A., Luis A. Ladino, Heike Wex, Yvonne Boose, Monika Burkert-Kohn, Daniel J. Cziczo, and Martina Krämer. 'Overview of Ice Nucleating Particles', *Meteor. Monogr.*, 58: 1.1-1.33. 2017.
- 10 Karagüzel, C., M. F. Can, E. Sönmez, and M. S. Çelik. 'Effect of electrolyte on surface free energy components of feldspar minerals using thin-layer wicking method', *J. Colloid Interface Sci.*, 285: 192-200. 2005.
- Kiselev, Alexei, Felix Bachmann, Philipp Pedevilla, Stephen J. Cox, Angelos Michaelides, Dagmar Gerthsen, and Thomas Leisner. 'Active sites in heterogeneous ice nucleation—the example of K-rich feldspars', *Science*. 2016.
- Kodera, N., D. Yamamoto, R. Ishikawa, and T. Ando. 'Video imaging of walking myosin V by high-speed atomic force microscopy', *Nature*, 468: 72-76. 2010.
- 15 Koop, Thomas, and Natalie Mahowald. 'Atmospheric science: The seeds of ice in clouds', *Nature*, 498: 302-03. 2013.
- Kreder, M. J., J. Alvarenga, P. Kim, and J. Aizenberg. 'Design of anti-icing surfaces: smooth, textured or slippery?'. *Nat. Rev. Mater.*, 1: 15. 2016.
- Lau, K. M., and H. T. Wu. 'Warm rain processes over tropical oceans and climate implications', *Geophys. Res. Lett.*, 30: 5. 2003.
- 20 Lohmann, U., and J. Feichter. 'Global indirect aerosol effects: a review', *Atmos. Chem. Phys.*, 5: 715-37. 2005.
- Marcilli, C. 'Deposition nucleation viewed as homogeneous or immersion freezing in pores and cavities', *Atmos. Chem. Phys.*, 14: 2071-104. 2014.
- Moosavi, A., M. Rauscher, and S. Dietrich. 'Motion of nanodroplets near edges and wedges', *Phys. Rev. Lett.*, 97: 4. 2006.
- Pach, E., and A. Verdaguer. 'Pores Dominate Ice Nucleation on Feldspars'. *J. Phys. Chem. C*, 123: 20998-1004. 2019.
- 25 Payton, O. D., L. Picco, and T. B. Scott. 'High-speed atomic force microscopy for materials science', *Int. Mater. Rev.*, 61: 473-94. 2016.
- Picco, L. M., P. G. Dunton, A. Ulcinas, D. J. Engledew, O. Hoshi, T. Ushiki, and M. J. Miles. 'High-speed AFM of human chromosomes in liquid', *Nanotechnology*, 19. 2008.
- Pruppacher, H. R., and J. D. Klett. *Microphysics of clouds and precipitation* (Kluwer Academic Publishers, Dordrecht, The Netherlands). 1997.
- 30 Pyne, A., W. Marks, L. M. Picco, P. G. Dunton, A. Ulcinas, M. E. Barbour, S. B. Jones, J. Gimzewski, and M. J. Miles. 'High-speed atomic force microscopy of dental enamel dissolution in citric acid', *Arch. Histol. Cytol.*, 72: 209-15. 2009.
- Rogers, R.R., and M.K. Yau. *A short course in cloud physics* (Pergamon Press: Oxford). 1989.
- Russell-Pavier, F. S., L. Picco, J. C. C. Day, N. R. Shatil, A. Yacoot, and O. D. Payton. 'Hi-Fi AFM': high-speed contact mode atomic force microscopy with optical pickups', *Meas. Sci. Technol.*, 29. 2018.
- 35 Rykaczewski, K., M. R. Henry, and A. G. Fedorov. 'Electron beam induced deposition of residual hydrocarbons in the presence of a multiwall carbon nanotube', *Appl. Phys. Lett.*, 95. 2009.
- Seemann, R., M. Brinkmann, S. Herminghaus, K. Khare, B. M. Law, S. McBride, K. Kostourou, E. Gurevich, S. Bommer, C. Herrmann, and D. Michler. 'Wetting morphologies and their transitions in grooved substrates', *J. Phys.-Condes. Matter*, 23: 16. 2011.
- 40 Uchihashi, T., R. Iino, T. Ando, and H. Noji. 'High-Speed Atomic Force Microscopy Reveals Rotary Catalysis of Rotorless F-1-ATPase', *Science*, 333: 755-58. 2011.
- Vali, G., P. J. DeMott, O. Mohler, and T. F. Whale. 'Technical Note: A proposal for ice nucleation terminology', *Atmos. Chem. Phys.*, 15: 10263-70. 2015.
- 45 Vergara-Temprado, J., M. A. Holden, T. R. Orton, D. O'Sullivan, N. S. Umo, J. Browse, C. Reddington, M. T. Baeza-Romero, J. M. Jones, A. Lea-Langton, A. Williams, K. S. Carslaw, and B. J. Murray. 'Is Black Carbon an Unimportant Ice-Nucleating Particle in Mixed-Phase Clouds?'. *J Geophys Res Atmos*, 123: 4273-83. 2018.
- Wang, Bingbing, Daniel A. Knopf, Swarup China, Bruce W. Arey, Tristan H. Harder, Mary K. Gilles, and Alexander Laskin. 'Direct observation of ice nucleation events on individual atmospheric particles', *Phys. Chem. Chem. Phys.*, 18: 29721-31. 2016.
- 50 Wang, Y., X. Liu, C. Hoose, and B. Wang. 'Different contact angle distributions for heterogeneous ice nucleation in the Community Atmospheric Model version 5', *Atmos. Chem. Phys.*, 14: 10411-30. 2014.
- Welti, A., Z. A. Kanji, F. Luond, O. Stetzer, and U. Lohmann. 'Exploring the Mechanisms of Ice Nucleation on Kaolinite: From Deposition Nucleation to Condensation Freezing', *J. Atmos. Sci.*, 71: 16-36. 2014.
- 55 Yamashita, H., K. Voitchovsky, T. Uchihashi, S. A. Contera, J. F. Ryan, and T. Ando. 'Dynamics of bacteriorhodopsin 2D crystal observed by high-speed atomic force microscopy', *J Struct Biol*, 167: 153-58. 2009.
- Yang, F., O. Cruikshank, W. L. He, A. Kostinski, and R. A. Shaw. 'Nonthermal ice nucleation observed at distorted contact lines of supercooled water drops', *Phys. Rev. E*, 97. 2018.
- Yang, F., R. A. Shaw, C. W. Gurganus, S. K. Chong, and Y. K. Yap. 'Ice nucleation at the contact line triggered by transient electrowetting fields', *Appl. Phys. Lett.*, 107. 2015.
- 60



5 **Figure 1:** Experimental Setup. (a) The 3-port fluid cell. The port design separates the humid and cold gases before injection into the cell, which are then mixed to form a cold humid atmosphere just before entry to the sample volume. (b) The overall setup is built around an existing AFM  
 10 (8) with top-down optics (2). Dry nitrogen is divided into cold and humid streams. The cold stream is nitrogen gas cooled in a liquid nitrogen-filled dewar (3), mixed at (4) with a dosage of room temperature nitrogen gas varied by (5). The total flow rate of the cold stream is unchanged, only the proportions of cold and warm flows are adjusted. The humid stream is generated by flowing nitrogen through a bubbler filled with water  
 15 (6). The humid gas leaving the bubbler is directed by a 3-way valve towards either a humidity sensor (7), or to the sample cell. The cold and humid streams of nitrogen gas enter an acrylic bell jar which houses the AFM scanner with a cellophane bellows bridging the optical objective (2) to the top rim of the jar. The humid stream enters one port of the sample cell while the cold stream is divided to cool the underside of the sample, by way of a copper stand-off stage (9), and flow a smaller proportion into the other port of the sample cell. The temperature of the underside of the sample stage and the gas exiting the cell are measured with thermistors. The decimal values next to flow line segments are flow rates for those segments in L/min.

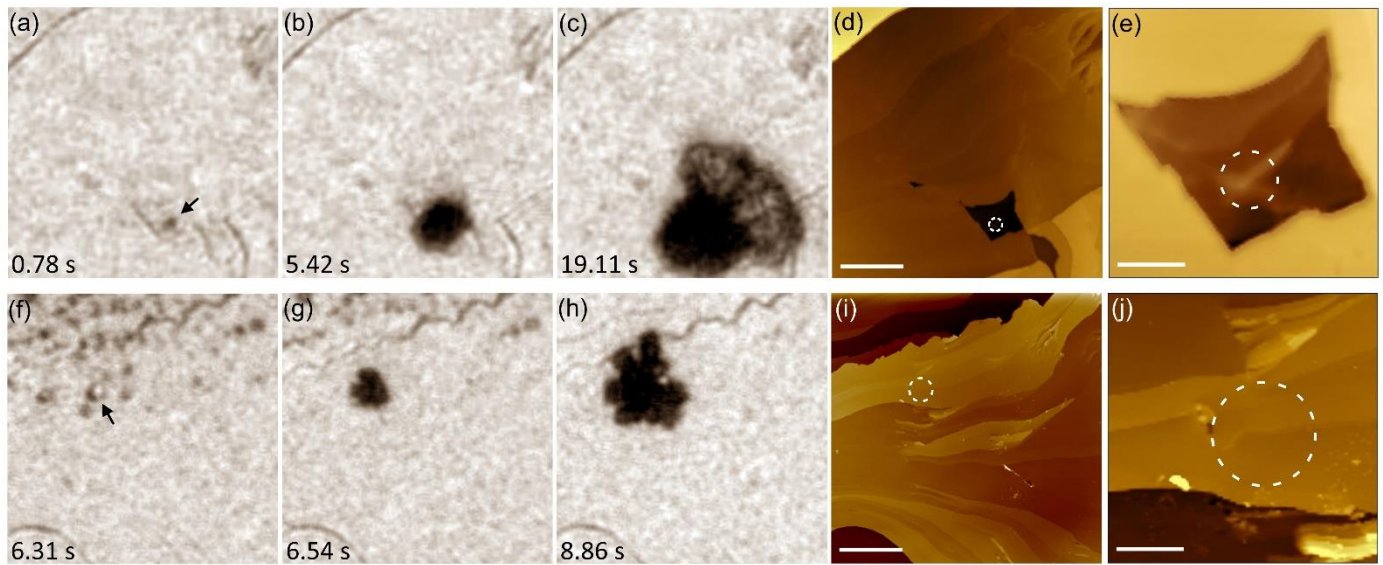


**Figure 2:** Colocating isolated nucleation events at  $-3029.5 \pm 0.5$  C to AFM topography. (a)-(c) Three frames of an ice crystal nucleating and growing under  $AH_{in} = 0.3840 \pm 0.08$  g/m<sup>3</sup>. (d) AFM image of the same location in a-c) with dashed circle around the area of nucleation. Scale bar 20 μm. (e) Expanded view of a portion of panel (d) showing a small protrusion within a larger pit. Scale bar 5 μm. (f)-(h) Frames taken under  $AH_{in} = 0.4548 \pm 0.08$  g/m<sup>3</sup> which show a collection of droplets on the surface in panel (f). The arrow points to the droplet which initiates an ice crystal. (i) AFM of the same area as in (f)-(h) with a circle around the original droplet in (f). Scale bar 20 μm. (j) Expanded view of panel (i). Scale bar 5 μm. Time stamps in lower left corner of optical frames are relative to the start time of their respective movies, however the time when water vapor fills the cell is not measured with significant precision. Accompanying videos can be found at (Friddle and Thürmer 2019b).

10

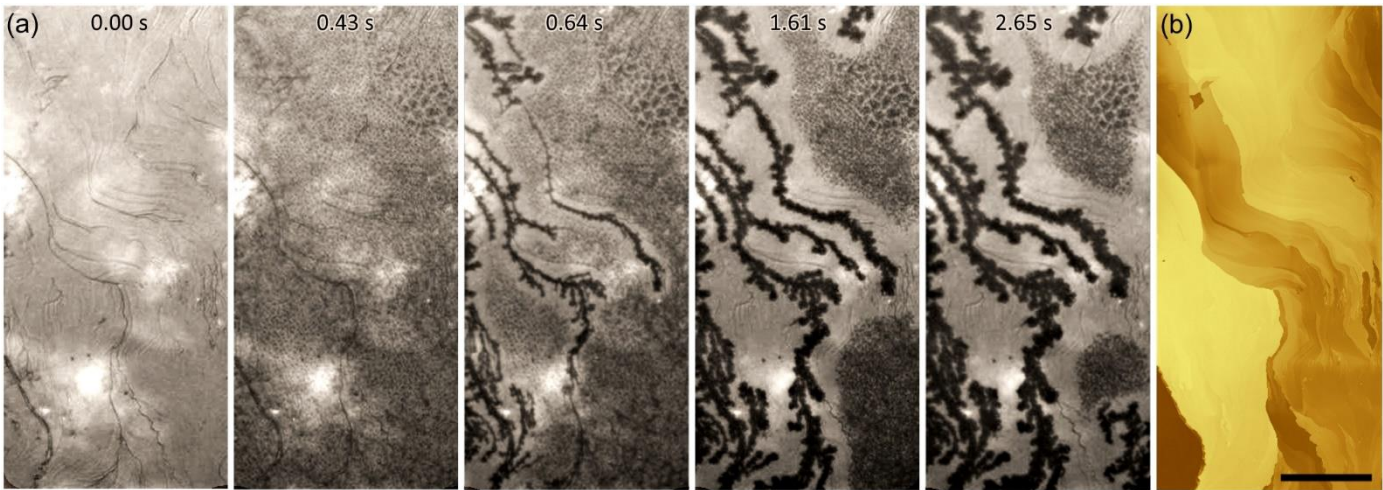


**Figure 3:** Ice growth on the feldspar surface at  $-3029.5 \pm 0.5$  C and  $AH_{in} = 0.7580 \pm 0.08$  g/m<sup>3</sup>. (a) Video frames at the noted times show the progression from a dry surface (0.00 s), to surface water condensation (0.43 s), and finally to propagation of ice across the surface. From 0.64 – 2.65 s the denuded zone (dehydrated halo) around the ice filaments expands with ice growth. (b) AFM mosaic of the same area as in a) where lighter color indicates higher surface topography. Note the prominent step edges follow the same path as many of the ice filaments. Scale bar 100 μm. Accompanying video can be found at (Friddle and Thürmer 2019b).

15

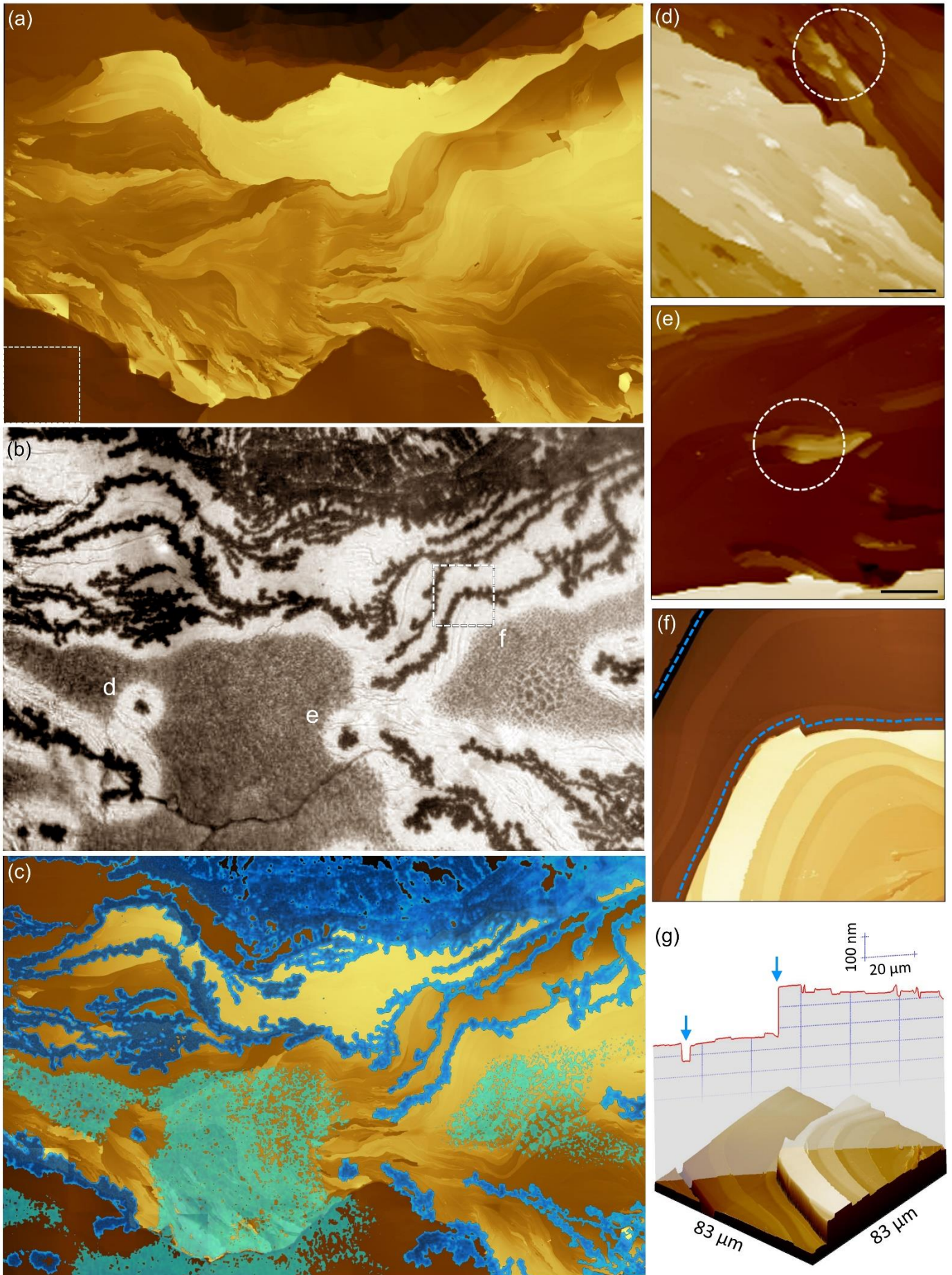


**Figure 4:** Wide field of view collocation of AFM data and optical video of ice growth at  $-3029.5 \pm 0.5$  C and  $AH_{in} = 0.7580 \pm 0.08$  g/m<sup>3</sup>. **(a)** A mosaic composed of 54 individual AFM images stitched together to form a topographical map spanning  $750 \times 570$   $\mu\text{m}^2$ . The dashed box in the lower left represents the  $100 \times 100$   $\mu\text{m}^2$  size of each individual AFM image. Brighter color represents higher topography. **(b)** An optical video frame captured over the same area as in a) showing ice growth. Three locations of interest are marked on the optical image (d, e, and f) and AFM images corresponding to their locations are shown in the panels at the right with the same labels. **(c)** The optical image in panel (b) is thresholded and false-colored, then overlaid on the AFM data shown in panel (a). The resulting overlay demonstrates the preference of ice formation along prominent step edges. **(d),(e)** Two example regions where ice nucleated on the surface and grew as isolated crystals without propagating across steps. Dashed circles enclose the locations where ice nucleation occurred. Scale bars are 5  $\mu\text{m}$ . **(f)** Planar and **(g)** 3D view of the region marked f in panel (b). Dashed lines in (f) represent the path followed by ice, and the arrows in the height profile in (g) mark locations of ice formation. Video data accompanying figure 4b can be found at (Friddle and Thürmer 2019b).

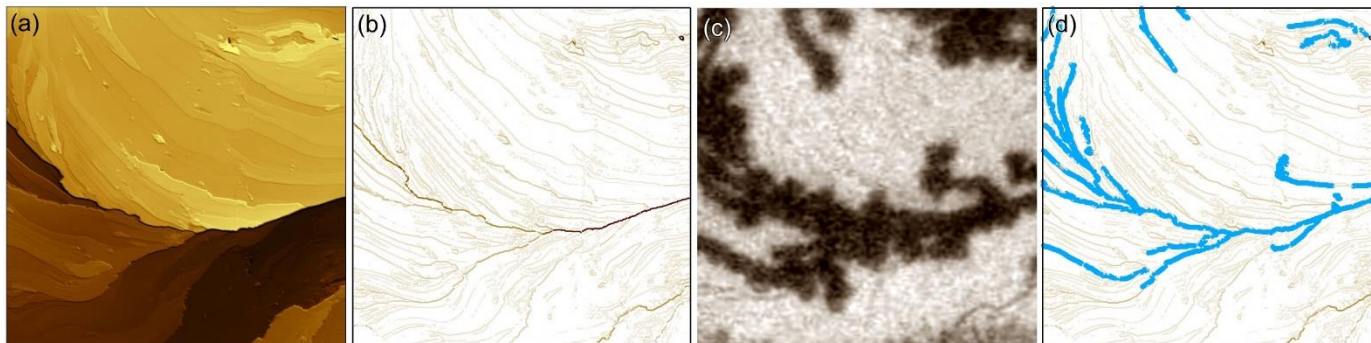
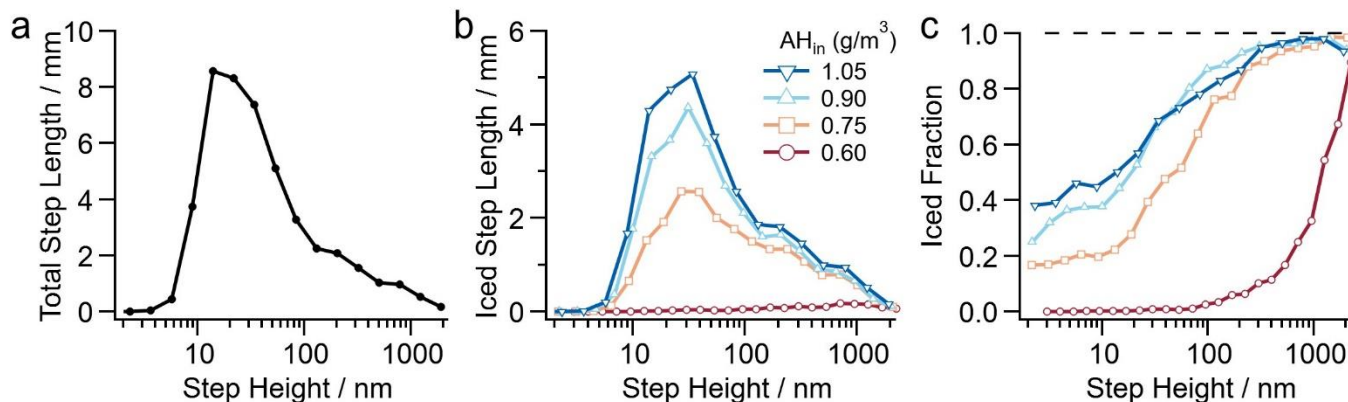


**Figure 5:** Processing video and AFM data into step-height statistics. An AFM image **(a)** is converted to an image of step-heights **(b)** and compared to the corresponding optical image of ice formation **(c)**. The step-height image in panel (b) is interactive in that the traces corresponding to ice-covered step segments can be selected by mouse click, shown as blue traces in **(d)**.



20

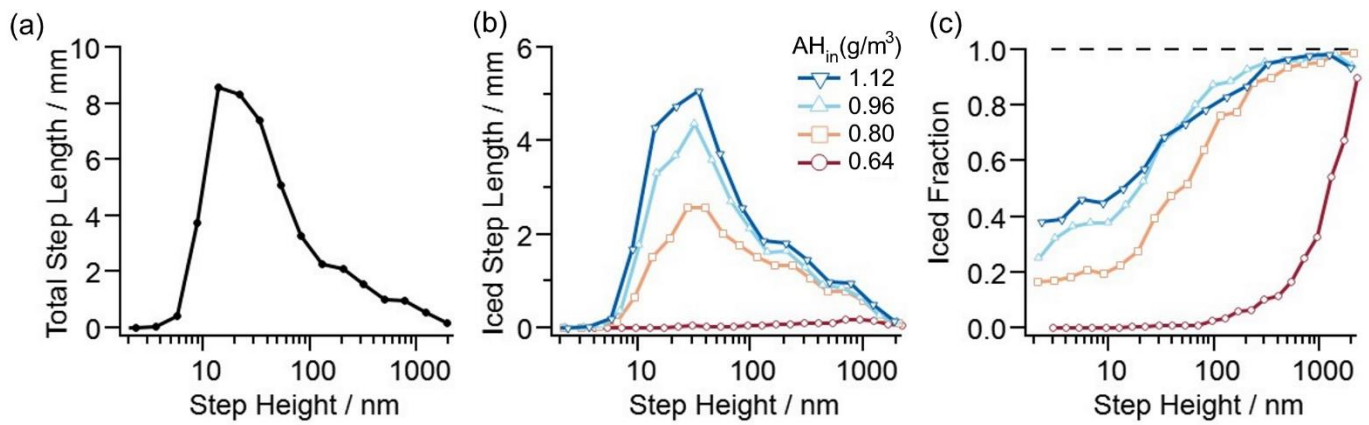


**Figure 6:** Step-height statistics. (a) Histogram of *all* step heights as measured by the total length of *all* steps within a step-height bin. (b) Histogram of step heights as measured by the total length of *iced* steps within a step-height bin. The histograms evaluate 15 images, each image covering  $100 \times 100 \mu\text{m}^2$ . The bins are logarithmically spaced, and binning for each step height is counted up as the sum of step-edge lengths. (c) Probability of finding ice on a step of a given height, computed as the total length of iced steps within a step-height bin divided by the total length of *all* steps (within the same step-height bin). The data show that increasing humidity shifts the distribution to the left, thus increasing the probability of finding ice on smaller step heights. Fluctuations in the ice fraction curves, particularly at high  $AH_{in}$  and large steps, reflect the random dehydration of some larger step heights which are present in far fewer numbers than smaller step heights.